Finite Element Analysis of Bearing Capacity of Concrete-Filled Double-Steel Tube Brace-Column K-Joints Under Monotonic Loading

Sadaf Qasim Shekhler, Taghi Mofid*

Department of Civil Engineering, Urmia University of Technology, Urmia, Iran

* Corresponding author: mofid.t@uut.ac.ir

Abstract:

The application of concrete-filled double-steel tube (CFDST) joints in structural engineering has received great attention due to their high load-bearing capacity, excellent ductility, and favorable seismic performance. In this study, the load-bearing capacity of CFDST brace-column K-joints under monotonic loading was examined using the finite element method via Abaqus. The numerical results were successfully validated against experimental and analytical models from the literature, showing good agreement in load-displacement response and failure modes. A parametric study was conducted to investigate the effects of brace diameter, column-brace angle, and sandwiched concrete between the inner and outer steel tubes on the failure behavior and overall capacity of the K-joint. Results indicate that the load-bearing capacity decreases with increasing brace diameter and with increasing brace-column angle. Models with sandwiched concrete exhibited significantly higher peak loads compared to hollow joints, due to the composite action enhancing stiffness and delaying local buckling. The maximum load resisted by the CFDST K-joint reached 2755 kN, representing a 156% increase over the joint without concrete. Although concrete infill substantially improves stiffness and capacity, the compressive strength level of the concrete plays a negligible role; thus, even low-strength concrete can be effectively used. Comparison of ultimate displacements also revealed that concrete-filled models possess much greater ductility than hollow ones. The novelty of this study lies in the simultaneous parametric investigation of brace diameter, brace-to-column angle, and concrete infill on the load-bearing capacity of CFDST K-joints using a validated finite element model.

Keywords:

CFDST Joint ; Bearing capacity ; Monotonic loading ; Finite element ; Abaqus.

1. Introduction

Joints play a vital role in structural systems, acting as interfaces between different structural elements. The design and performance of these connections significantly affect the overall performance, stability, and integrity of the structure. These connections facilitate the transfer of loads between structural elements and ensure that forces are distributed evenly throughout the structure. In particular, steel tubular connections are critical components in engineering, especially in the construction of buildings, bridges, offshore structures, stadiums, refineries, and many other infrastructures [1-6]. These members are designed to connect tubular sections consisting of columns, braces, and other elements, providing the overall strength and stability of the structure. On the other hand, the use of concrete-steel composite joints in structural engineering construction has received more attention due to the unique characteristics of this type of component, which is a result of combining the capabilities of concrete and steel. One of the common composite joints is concrete-filled steel tubes (CFSTs). These joints are a group of structural members that consist of hollow steel tubes filled with concrete. In this case, both steel and concrete materials work together to create several structural advantages. In this regard, concrete increases the resistance of the steel tube to local buckling, while the steel tube encloses the concrete, thus increasing its compressive strength. However, the main problem with CFST brace-column joints is the weakness at the intersection of the brace and the main column. At this point, punching shear causes premature failure of the connection or local buckling of the main member. Several methods such as the use of doubler/collar reinforcement plates or increasing the thickness of the steel wall at the connection zone have been proposed; nevertheless, the use of these plates in some cases is neither economical nor prevents local buckling of the main column and overall buckling of the composite connection. To solve this problem, concrete-filled double-steel tubes (CFDSTs) consisting of concentric inner steel shell, an outer steel shell, and concrete filled between the two shells have been proposed in recent years. In this case, the buckling of the connection is transferred from the main column to the bracing member and the overall stability of the connection is improved. The inner shell or outer shell can be circular, rectangular, or square hollow sections. In addition, the outer steel shell can be made of carbon steel or stainless steel. CFDST structures inherit the advantages of conventional CFST structures, including high strength, good ductility and durability, high fire resistance, and favorable constructability [7-14].

In addition, due to their unique cross-sectional configuration, CFDSTs have lighter weight, higher bending stiffness, and better cyclic performance than conventional CFST. As a result, CFDST can offer lower concrete consumption and construction costs. In addition, steel tubes can act as concrete forms during construction. These tubes can also bear a significant amount of construction load before concrete is pumped, which leads to higher construction efficiency.

Despite the growing application of concrete-filled double-skin steel tubular (CFDST) members in modern structural engineering, the behaviour of CFDST K-joints under monotonic loading has received limited attention in the literature. Most existing studies have focused on conventional CFST joints or on CFDST members under axial or cyclic loading, while systematic parametric investigations on K-joints – particularly those addressing the combined effects of brace diameter, brace-to-column angle, and concrete infill – remain scarce. Moreover, the underlying mechanical mechanisms governing the failure modes and load transfer in these joints are not yet fully understood. This research gap hinders the development of reliable design guidelines for CFDST K-joints in critical applications such as offshore platforms, refinery piping systems, transmission towers, and bridge piers, where these connections are frequently employed. Advanced numerical techniques such as XFEM have also been effectively used to model crack propagation and retrofitting in concrete structures [15, 16]. The present study aims to fill this gap by developing a validated three-dimensional finite element model of CFDST K-joints and conducting a comprehensive parametric analysis to quantify the influence of key geometric and material parameters on the joint's load-bearing capacity, stiffness, ductility, and failure mode. The findings provide new insights into the structural performance of these joints and offer practical recommendations for their design and strengthening, particularly regarding the beneficial role of sandwiched concrete in enhancing capacity and ductility.

Although several studies have investigated the behaviour of concrete-filled steel tubular (CFST) joints and CFDST members under various loading conditions, a comprehensive parametric investigation on CFDST K-joints that simultaneously considers the effects of brace diameter, brace-to-column angle, and concrete infill is still lacking. Most existing research has focused on either axial behaviour of CFDST columns or the performance of T-type and X-type joints, while the combined influence of these key geometric and material parameters on the load-bearing capacity, failure mode, and ductility of K-joints remains unexplored. Furthermore, the nonlinear interaction between the steel tubes and the sandwiched concrete in these joints has not been fully addressed in previous numerical studies. This research gap limits the development of reliable design recommendations for CFDST K-joints in practical applications. The present study aims to fill this gap by developing a validated three-dimensional finite element model and conducting a systematic parametric analysis to quantify the individual and combined effects of the aforementioned parameters on the structural performance of CFDST K-joints under monotonic loading.

2. Literature Review

Although CFDST elements are a new generation of composite members, there is a great interest among engineers and researchers to investigate and apply these types of elements in various engineering structures. In addition, the existence of special configurations of these elements, such as CFDST joints with a geometric shape of K, especially in structures such as stadiums, refineries, offshore platforms, bridge piers, power transmission towers and electricity grid structures, has led many researchers to focus on how these members perform under different loadings and achieve higher load capacity and optimal states in these types of joints. In this regard, Xia et al. [17] studied the stress concentration coefficients (SCFs) in circular hollow-section (CHS) joints and CFDST K-joints. Accordingly, the effects of key geometric parameters, such as the brace-to-column diameter ratio β, the column diameter-to-thickness ratio γ, the brace-to-column wall thickness ratio τ, the brace angle θ, and the hollow ratio ζ, on the distribution and key locations of SCFs were discussed. The results showed that the sandwiched concrete could effectively reduce SCFs along the weld. When the hollow ratio was reduced from 0.915 to 0.317, the SCFs were mitigated by 77.2%. It was also noted that the SCF reduction rate was contingent on γ and θ. Interestingly, the distribution of SCFs were similar for joints of the same type but with different geometric configurations. Naghipour et al. [18] presented a finite element modeling analysis to investigate the ultimate bearing capacity of circular and square CFDST T-joints. A set of 24 joint specimens were modeled in Abaqus software. According to the results, the circular CFDST T-joints showed higher stress-bearing capacity compared to the square-section joints. This behavior was attributed to the better confinement of the concrete in the circular tubes and consequently the higher load-bearing capacity of the entire connection. Li et al. [19] investigated the static performance of chord-brace KK-joints with CHS columns. the main failure mode in finite element modeling was identified as punching shear at the connection of the brace members to the main chord. It was realized that filling the chord with the concrete effectively delayed the plastic deformation of the joint wall, leading to an improvement in the ultimate bearing capacity and preventing the yielding of the column wall in the compression brace. Huang et al. [20] conducted a laboratory study on CFST truss K-joint. It was found that the dominant failure mode and the strength decay cause was punching shear at the weld of the braced member to the main column. Punching shear occurred when high shear stresses were generated around the stress concentration area, often leading to cracking and eventual failure of the joint. Witteck et al. [21] conducted an experimental study on the performance of novel CFDST columns with high-performance building materials under uniform and cyclic loading. According to the results, in general, CFDST has a comparable shape of hysteresis curves to CFST, which indicates that the CFDST column type has a similar overall cyclic response to the CFST type. Also, all specimens showed symmetrical and ductile behavior during cyclic loading. Nonetheless, CFDST columns showed a more complete hysteresis curve compared to CFST, indicating a better energy dissipation capacity of CFDST compared to CFST. Accordingly, each column under repeated loading at the same displacement experiences material softening. However, it is interesting to note that the use of a high-strength inner tube increased the stiffness and lateral load capacity of the CFDST specimen compared to the CFST. However, when comparing the CFST and CFDST specimens, the effect of high-strength concrete on lateral load capacity was low. Thus, concrete strength played a minor role in improving the load capacity than the shell steel. Zhao et al. [22] conducted experimental and numerical studies on the performance of CFDST columns and beams with inner tube made of carbon steel and outer shell made of stainless steel. Finite element models were also developed and validated with experimental results. In the slender columns, global buckling with large lateral deflection was observed. However, local buckling at mid-section height was not observed due to the presence of sandwiched concrete. In addition, similar failure patterns were observed in conventional CFST and CFDST columns with carbon outer tube. It was noted that there was no significant difference in the failure pattern between specimens with different hollow ratios. In contrast to the hollow columns, the CFDST column specimens showed negligible local buckling on the compression side. When examining the concrete inside the beam specimens, the sandwiched concrete between the tubes remained intact while tensile cracks occurred mainly at the bottom of the cross section in the middle of the beam span. According to the finite element results, for columns with a diameter of 600 mm, increasing the hollow ratio had a negligible effect on the ultimate capacity. Columns with a hollow ratio of 0.7 showed the lowest bearing capacity, while the highest ultimate strength was recorded at a hollow ratio of 0.5. Furthermore, the bearing capacity decreased with increasing load eccentricity ratio, and increased with increasing yield stress of the outer steel tube and concrete strength. It was observed that the strength of the inner steel tube has a slight effect on the ultimate strength of columns. This is mainly because the flexural strength is slightly affected by the change in the strength of the inner steel tube located near the neutral axis. In 2025, Yang et al. [23] conducted a finite element study of the performance of CFDST column bases derived from load-bearing beams under axial and lateral compressive loading in terms of the design methods. Three failure patterns of (1) punching shear failure; (2) flexural failure of the CFDST column; and (3) pullout failure of the column base were identified. The lateral deformation of the column base initially consisted of rotational and flexural components. Subsequently, the

CFDST column underwent significant external buckling and formed plastic hinges with increasing load level. At this stage, the flexural deformation was dominant, accounting for approximately 60% of the total deformation. Asadollahi et al. [24] studied the bearing capacity of CFDSTs filled with concrete inside and outside the inner tube using the Abaqus software. The load-moment interaction capacity curves were obtained and the effect of geometric and mechanical parameters were investigated. Accordingly, the CFDST capacity increased linearly with increasing the strength of the inner and outer concrete. Also, the capacity increased with increasing the yield stress of the steel. However, the effect of increasing the yield stress of the outer tube was much greater than that of the inner tube. In addition, considering the confinement of the concrete in the modeling process had no effect on CFDST moment and had a negligible effect on the axial load. In addition to studies on CFDST and CFST joints, extensive experimental investigations have been conducted on the mechanical behavior of reinforced concrete (RC) elements under various loading conditions, including post-earthquake loading, cyclic degradation, and repeated loadings. These studies highlight the importance of understanding material degradation and failure mechanisms under different load histories, which is also relevant to the performance of composite members such as CFDST joints under monotonic and cyclic loading [25-27].

3. Numerical Analysis Method

3.1 Model Geometry and Specifications

In this research, the load-bearing capacity of a CFDST K-joint under monotonic loading was studied using the finite element method and the Abaqus software. The schematic of the K-joint configuration is illustrated in Figure (1). A total of eight K-joint models with column length L=1000 mm, the length of the compression and tension braces l=430 mm, the distance between the braces g=3 mm, the angle between column and brace θ=45° and 60°, the diameter of the outer column tube D_o=140 mm, the diameter of the inner column tube D_i=85 mm, the diameter of the bracing member d_1=d_2=46 mm and 85 mm, the wall thickness of the column tubes T_o=T_i=3.6 mm, and the wall diameter of the bracing steel tube t_1=t_2=2.8 mm were created and examined in the software. It should be noted that the steel tubes in the CFDST joint column member are placed concentrically and with the same length relative to each other.

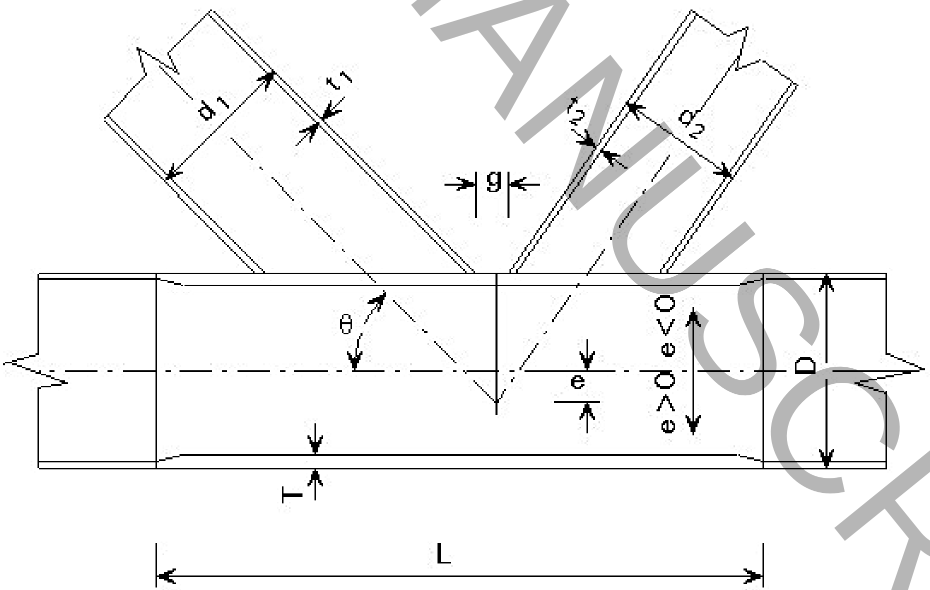

Figure 1. Schematic of the K-joint configuration

The properties of the ST37 steel tube were modeled as isotropic and fully elastic-plastic. The density, yield strength, elastic modulus, and Poisson's ratio of steel were determined to be 7850 kg/m^3, 360 MPa, 210 GPa, and 0.3, respectively. Based on Figure (2), a linear model for the joint supports and a trilinear model were used to simulate the stress-strain curve of the steel, which was designed according to the von Mises yield criterion characterizing isotropic hardening. Also, the constant *a* in this stress-strain curve was considered to be 0.9%. The value of a=0.9% is adopted following the recommended strain-hardening parameter for mild steel (ST37) in ABAQUS, as suggested by Han et al., 2014 [28].

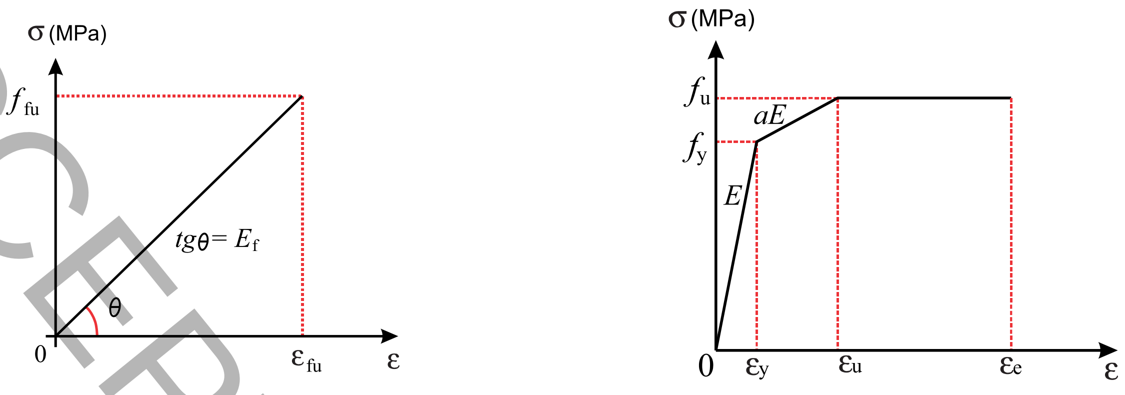

(a) (b)

Figure 2. Stress-strain curves for (a) support steel and (b) tube steel in modeling CFDST K-joint

Given the brittle behavior of concrete, concrete damage plasticity (CDP) of Lubliner was used to model the concrete. Figure (3) shows the stress-strain behavior of the modeled concrete in tension and compression. Also, the behavior of the concrete material was considered isotropic. The interaction between steel and concrete was determined as a hard contact in the normal direction and penalty friction in the tangential direction. The mechanical properties of the concrete used in this study were 24 MPa for the 28-day compressive strength, 27 GPa for the Young's modulus, 0.18 for the Poisson's ratio, and 1890 kg/m^3 for the density.

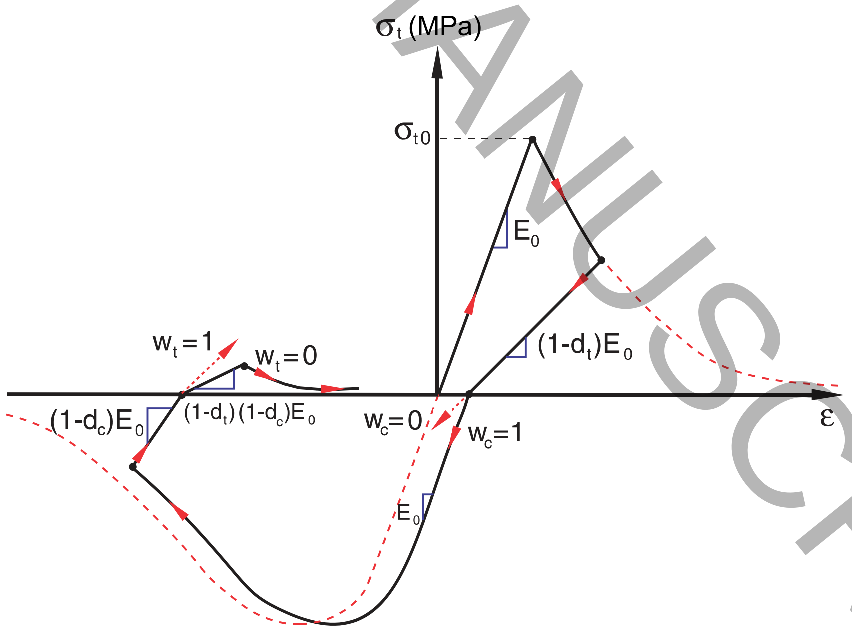

Figure 3. Concrete stress-strain behavior in tension and compression

Given that the K-joint under investigation is subjected to static loading .The Coulomb friction coefficient between the steel and concrete surfaces in contact was taken to be 0.6. Also, the elements do not allow penetration between the two surfaces under pressure. Displacement/rotation boundary condition sets of U_2=0 and U_2=U_3=0 were applied to the brace members on the right and left side, as shown in Figure (4). In addition, a compressive load of 1500 kN was applied to the main column member. A displacement-controlled loading scheme with a rate of 0.5 mm/s was applied to the braces. Also, a mesh size of 25 mm and the type of structured mesh technique and hexagonal element shape with curvature control of the element surfaces were used.

Owing to the symmetrical configuration of the K-joint and equal loading on both braces, the eccentricity effects are negligible and therefore ignored.

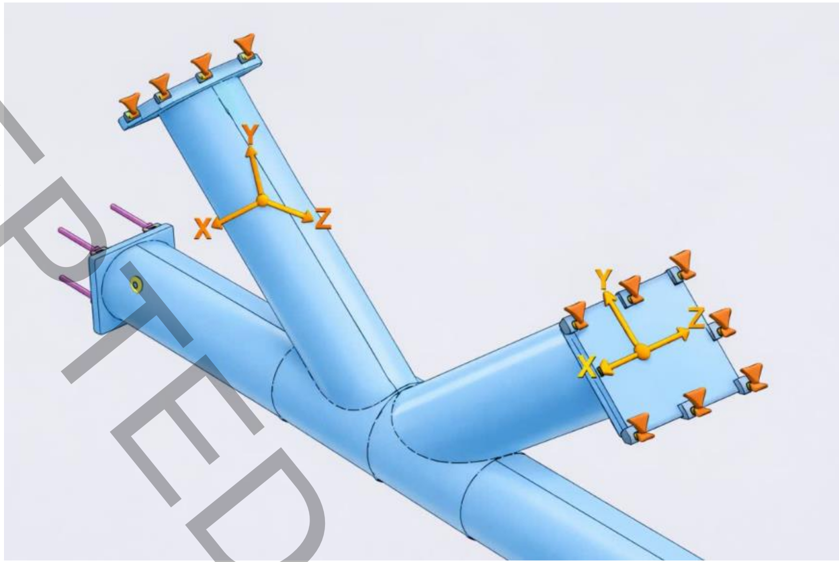

Figure 4. CFDST K-joint loading and boundary conditions

The equivalent section method was employed to estimate the compound elastic stiffnesses of the CFDST section. The axial stiffness (*EA*), flexural stiffness (*EI*), and shear stiffness (*GA*) were calculated by combining the contributions of the outer steel tube, inner steel tube, and sandwiched concrete as follows:

$$EA = Es\,As + Ec\,Ac \quad (1)$$

$$EI = Es\,Is + Ec\,Ic \quad (2)$$

$$GA = Gs\,As + Gc\,Ac \quad (3)$$

where E and G are the elastic and shear moduli, A is the cross-sectional area, I is the second moment of area, and the subscripts ss and cc denote steel and concrete, respectively.

To provide a clear and comprehensive justification for all modeling assumptions, the key material and interaction parameters employed in the numerical simulations are summarized in Table 2, along with their respective values and supporting references.

Table 2. Summary of material and interaction parameters for numerical modeling.

Parameter	**Value**	**Reference / Justification**
Steel material model	Isotropic elastic–plastic with von Mises yield criterion	ABAQUS default; standard for mild steel

Steel yield strength (F_y)	360 MPa	Manufacturer data for ST37 steel
Steel elastic modulus (E_s)	210 GPa	Standard value for structural steel
Steel Poisson's ratio (ν_s)	0.3	Standard value for structural steel
Steel density (ρ_s)	7850 kg/m³	Standard value for structural steel
Steel hardening parameter (a)	0.9%	Han et al. (2014)
Concrete material model	Concrete Damaged Plasticity (CDP)	Lubliner et al. (1989); ABAQUS manual
Concrete compressive strength (fc')	24 MPa	Experimental data from Hou et al. (2017)
Concrete elastic modulus (E_c)	27 GPa	ACI 318-19
Concrete Poisson's ratio (ν_c)	0.18	Standard value for normal-strength concrete
Concrete density (ρ_c)	1890 kg/m³	Experimental data
CDP – Dilation angle (ψ)	30°	ABAQUS manual; recommended for normal concrete
CDP – Eccentricity (ε)	0.1	ABAQUS default; Krätzig & Pölling (2004)
CDP – Ratio of biaxial to uniaxial strength ($\sigma b0/\sigma c0$)	1.16	Lubliner et al. (1989); ABAQUS default
CDP – Viscosity parameter (μ)	0.001	ABAQUS default; ensures convergence
Steel-concrete interaction – Normal behavior	Hard contact	ABAQUS default; no penetration allowed
Steel-concrete interaction – Tangential behavior	Penalty friction with $\mu = 0.6$	Standard for steel-concrete interfaces; Eurocode 4
Element type – Steel tubes	C3D8R (8-node brick, reduced integration)	Recommended for solid continuum elements in ABAQUS
Element type – Concrete infill	C3D8R (8-node brick, reduced integration)	Recommended for solid continuum elements in ABAQUS
Global mesh size	25 mm	Mesh convergence study
Refined mesh at joint intersection	10 mm	To capture stress concentration and local buckling
Loading protocol	Displacement-controlled, 0.5 mm/s	To capture post-peak behavior and avoid convergence issues
Boundary conditions – Left brace	U2 = 0	Symmetric loading configuration
Boundary conditions – Right brace	U2 = U3 = 0	Symmetric loading configuration
Boundary conditions – Column top	Compressive load of 1500 kN	As per experimental setup of Hou et al. (2017)

3.2 Mesh Sensitivity Analysis

To ensure the accuracy and reliability of the finite element results, a mesh sensitivity analysis was conducted prior to the parametric study. The objective was to select an appropriate mesh size that provides sufficient accuracy while maintaining reasonable computational cost. Five different global mesh sizes were examined: 15 mm, 20 mm, 25 mm, 30 mm, and 40 mm. All other modeling parameters, including material properties, boundary conditions, and loading protocol, were kept identical across the models. The reference model KJ0-45-46 was used for this convergence study. The ultimate load-bearing capacity obtained from each mesh size is summarized in Table 1. As the mesh is refined from 40 mm to 15 mm, the predicted ultimate load converges to a stable value. The 25-mm mesh predicts a load within 1.8% of the finest mesh (15 mm), while the 30-mm and 40-mm meshes show larger deviations of 4.2% and 8.7%, respectively. Moreover, the computational time for the 25-mm mesh is significantly lower than that for the 15-mm and 20-mm meshes, making it the most efficient choice. Based on the convergence study, a global mesh size of 25 mm was adopted for all models in the parametric investigation. Additionally, a finer mesh with an element size of 10 mm was applied locally at the brace-to-column intersection to accurately capture the stress concentration and local deformation in this critical region. The structured mesh technique with hexahedral elements (C3D8R) and curvature control was employed throughout the models. The selected mesh configuration provides a balance between computational efficiency and numerical accuracy, with a maximum error of less than 2% compared to the finest mesh.

Table 1. Mesh sensitivity analysis results for model KJ0-45-46.

Mesh size (mm)	Number of elements	Ultimate load (kN)	Error (%) vs. 15-mm mesh
15	38462	1318	—
20	21847	1309	0.7
25	13124	1294	1.8
30	8936	1263	4.2
40	5271	1203	8.7

3.3 Limit State and Failure Criteria

In the present study, the ultimate limit state (ULS) was adopted as the primary design criterion for evaluating the load-bearing capacity of the CFDST K-joints under monotonic loading. The ultimate load (peak load) was defined as the maximum load sustained by the joint prior to strength degradation, identified as the peak point on the load-displacement curve. Beyond this point, the joint experiences a significant loss of load-carrying capacity, indicating the onset of failure. The von Mises yield criterion was employed to assess the initiation of yielding in the steel components, with the yield stress of ST37 steel (360 MPa) used as the limiting threshold. Additionally, the equivalent plastic strain (PEEQ) was monitored throughout the analysis to detect localized plastic deformations and to distinguish between global joint failure and local material yielding at the brace-to-column intersection. This combined approach ensures that the reported ultimate capacities consistently represent the maximum load that the joint can sustain before undergoing progressive failure, while also providing insight into the underlying failure mechanisms.

4. Validation of Numerical Model

To validate the numerical results, the response of the K-joint under monotonic loading was investigated and compared with other experimental models available in the literature. Thus, the accuracy of the numerical results in this study was validated with experimental and analytical data in two separate studies by Hou et al. [29, 30]. Figure (5) shows the finite element results of the present study along with the experimental and analytic models examined by Hou et al. [29, 30]. According to the load-displacement curves, it is observed that the behavior of the models is in good agreement in terms of the initial stiffness, strength decay and up to the ultimate load point. The load associated with the yielding of the K-joint steel is also estimated with considerable accuracy. As observed in Figure 5, the elastic flexural stiffness predicted by the present finite element model is slightly lower than those of the analytical and experimental models reported by Hou et al. [29, 30]. This minor discrepancy can be attributed to several factors. First, in the numerical model, the steel–concrete interface is simulated using surface-based contact with frictional behavior ($\mu = 0.6$) in the tangential direction and hard contact in the normal direction, which allows for relative slip between the steel tube and the concrete infill. This realistic contact condition results in a more flexible response compared to the analytical model, which typically assumes perfect bonding (i.e., full composite action without slip) between the steel and concrete. Second, the experimental initial stiffness is often overestimated due to measurement uncertainties, instrumentation settlement, or minor gaps at loading platens during the early stages of loading, which are difficult to capture accurately in the physical tests. Despite this slight difference in initial stiffness, the overall load–displacement response, including the ultimate load, post-peak behavior, and failure displacement, shows good agreement between the FEM results and the experimental and analytical data. Therefore, the developed numerical model is considered sufficiently accurate for the parametric study presented in this paper.

According to AISC 360-16, the local buckling check for hollow tubes under axial compression requires $D/t \leq 0.11E/F_y$ For the present hollow column tubes (D/t=140/3.6=38.9), this limit is 0.11×(210000/360)=64.2, which confirms that the hollow sections satisfy the compactness requirement.
The stability factor (buckling reduction factor) for the axial compression member in the CFDST K-joint was determined according to AISC 360-16 provisions for composite columns. For the reference model, the calculated buckling reduction factor is 0.85, accounting for the enhanced stiffness provided by the concrete infill.

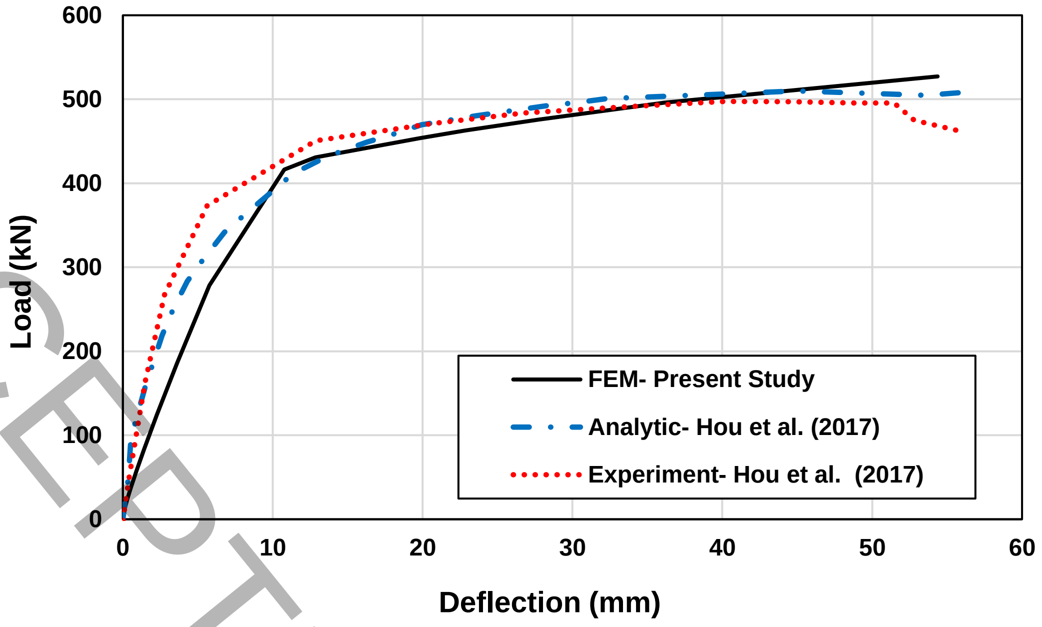

Figure 5. Comparison of finite element results in present study with experimental and analytic models by Hou et al. [29, 30]

It should be noted that the sudden loss of strength observed in the experimental load–displacement curve after the peak load is attributed to localized fracture at the weld toe or cracking of the concrete infill, which are not simulated in the present finite element model since no progressive damage or fracture criteria were incorporated. Both the numerical and experimental results are considered correct within their respective domains: the FEM accurately captures the pre-peak behavior, including initial stiffness, yielding, and ultimate load capacity, while the experimental curve reflects the post-peak response including fracture and strength degradation. Since the primary objective of this study is to evaluate the ultimate load-bearing capacity and the parametric influences on joint performance, the sudden post-peak drop in the experimental model does not affect the validity of the numerical model for the parametric investigation conducted herein.

5. Parametric Analysis Results

The parameters studied in this section include the effect of increasing the diameter of the bracing member (d_i) on the failure behavior and overall load-bearing capacity of the K-joint. Also, the change in the angle between the bracing member and the main column (θ) is investigated and its effect on the load-bearing capacity of the joint is evaluated. In addition, the effect of the presence and absence of core concrete (f'_c) in the K-joint and its contribution to the failure mode and load-bearing capacity of the entire joint is discussed. As such, two categories are examined in the modeling. In the first category, the space between the inner and outer concentric column tubes is modeled as empty, and the load-displacement behavior of the joint at the intersection point of the braces with the column at time steps Δ=0.02 is obtained from the software. In the second category, the space between the inner and outer steel tubes is filled with concrete with a compressive strength of 24 MPa in the modeling to evaluate the behavioral difference between the connection with and without sandwiched concrete. It should also be noted that in the parametric study of the K-joint, the diameter of the bracing steel tube was increased from d_i= 46 mm to 85 mm to examine the effect of the diameter change on the bearing capacity of the K-joint. Also, the angle between the bracing member and the column, which was changed from θ= 45° to 60° so that the effect of increasing the angle could be evaluated on the bearing capacity of the K-joint. Accordingly, the K-joint model KJ0-60-85, for instance, represents a model with no sandwiched concrete (f'_c=0), column-brace angle of θ=60°, and brace diameter of d=85 mm.

The load-displacement diagrams of K-joints for the first category models (with no sandwiched concrete) are plotted in Figure (6). As can be seen in Figure (6-a) for model KJ0-45-46, the curve increase with increasing the load and as a result of increase in displacement, until the point where the joint strength suddenly decreases at a displacement of 4.1 mm. At this point, the maximum load resisted by K-joint KJ0-45-46 is 854 kN. Regarding the reasons for this, it can be concluded that with a gradual increase in the applied load, the steel bracing member buckles and incurs a large pressure at the connection point to the main column member. This causes deformation and shrinkage of this part of the tube. With an increase in the amount of load, the joint progresses towards failure and the load-bearing capacity decreases significantly. As the loading continues, the joint strength increases slightly, but the displacement of the intersection point of the column and bracings increases sharply until the connection fails at a displacement of 81 mm and a load of 1314 kN. By carefully examining Figure (6-a), it can be seen that the curve has a small jump at a displacement of approximately 65 mm and then fails. This point actually shows the local failure of the column member, which is an undesirable mode of failure.

To examine the effect of increasing the diameter of the brace member from 46 mm to 85 mm, the load-displacement diagram of joint model KJ0-45-85 is shown in Figure (6-b). By comparing this diagram with joint KJ0-45-46, it can be concluded that the bearing capacity of the K-joint decreases with increasing the brace diameter. In this regard, the maximum bearing capacity of KJ0-45-85 is equal to 1077 kN, which occurs at a displacement of 48 mm. This represents a 12% reduction in the load-bearing capacity of the K-joint.

Furthermore, to examine the effect of change in brace-column angle from 45° to 60°, the load-displacement diagram of joint model KJ0-60-46 is demonstrated in Figure (6-c). By comparing this diagram with joint KJ0-45-46, it can be seen that increasing the angle reduces the load-bearing capacity. In this sense, the maximum bearing capacity of joint KJ0-60-46 is 982 kN at a displacement of 33 mm. This indicates a reduction of 9% in the load-bearing capacity of the CFDST K-joint. As a result, connections with a smaller angle have a higher bearing capacity. This can be related to the principle of superposition of forces, and subsequently, the higher contribution of brace members with the column to load-bearing capacity at smaller angles. It is reminded that smaller angle denotes for when the brace member is closer to the main column in terms of geometric position. It can also be seen in Figure (6-d) that joint model KJ0-60-85 has the lowest load capacity because it bears the highest brace diameter and angle. In order to better demonstrate the effect of change in brace diameter and chord-brace angle, the load-displacement curves for the first category are plotted in Figure (6-e) for the purpose of comparison.

Subsequently, the results of the second category of K-joints filled with concrete with a compressive strength of 24 MPa were discussed in terms of the overall load-bearing capacity of the CFDST K-joint. It is observed that the models with sandwiched concrete have higher peak loads, compared to models with no filler concrete. This is due to the contribution of concrete to the overall capacity increase of the K-joint. In this regard, the peak load of the specimens with concrete is more than twice as high as that of specimens without concrete. The load-displacement diagrams of K-joints for the second category models (with sandwiched concrete) are plotted in Figure (7). As can be seen in Figure (7-a), the maximum load resisted by K-joint KJ24-45-46 is 2755 kN at a displacement of 59 mm. This is indicative of a 156% increase in load capacity of the CFDST K-joint in comparison to the joint with no concrete modeling. In addition, the comparison of the ultimate displacement for the models without concrete shows that the ductility of these models is much lower than that of the models filled with concrete. In addition, comparing the results shows that although filling K-joints with concrete significantly increases the stiffness and overall capacity of the joint, the compressive strength level of the concrete plays a negligible role in this regard. Therefore, even low-strength concrete types can be used to strengthen these types of joints. According to Figure (7), the failure mode in concrete-filled joint models is either buckling of the brace member in compression or plastification of the column member steel at the column-brace intersection, which both are desirable modes of failure.

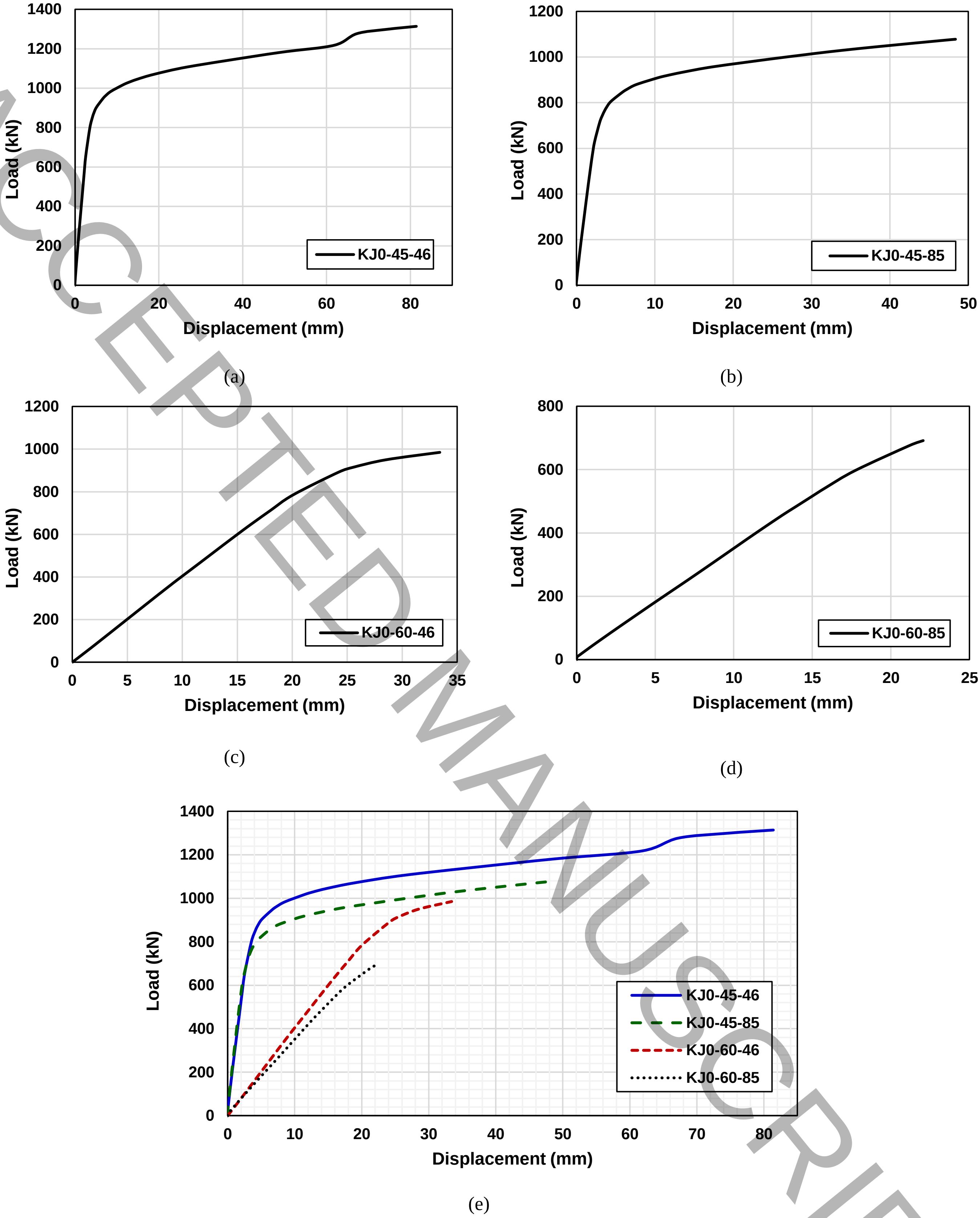

Figure 6. Load-displacement diagrams for K-joint models:
(a) KJ0-45-46, (b) KJ0-45-85, (c) KJ0-60-46, (d) KJ0-60-85, and (e) all

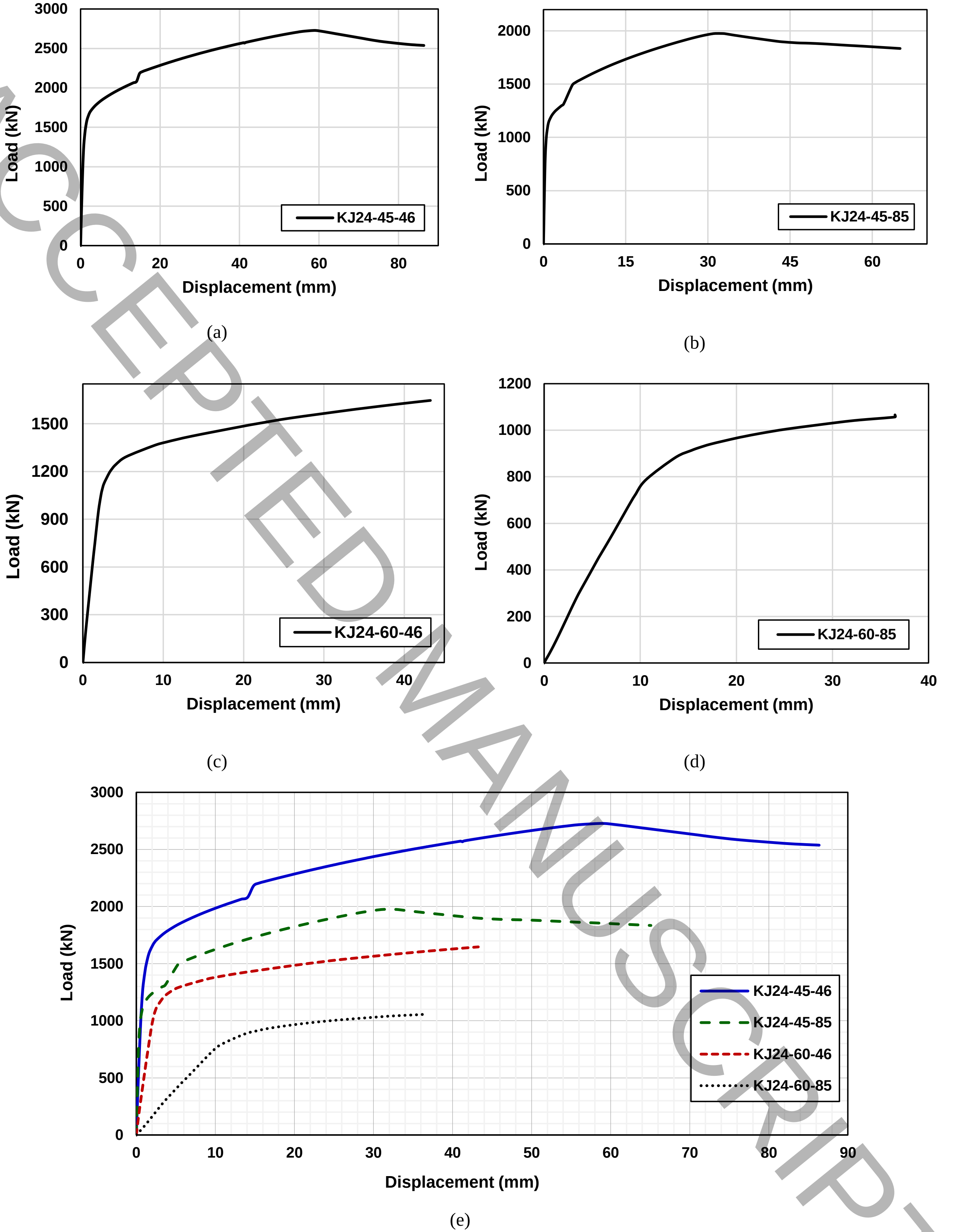

Figure 7. Load-displacement diagrams for K-joint models:
(a) KJ24-45-46, (b) KJ24-45-85, (c) KJ24-60-46, (d) KJ24-60-85, and (e) all

To provide a deeper understanding of the structural response of CFDST K-joints, a detailed mechanistic analysis was conducted by examining the load-displacement characteristics, deformation patterns, and the underlying physical mechanisms governing the failure modes. This analysis focuses on the influence of key geometric parameters, including brace diameter and brace-to-column angle, as well as the presence or absence of sandwiched concrete, on the joint capacity and failure behaviour.

5.1 Failure Mechanisms of Models without Concrete Infill

For the models without sandwiched concrete (KJ0 series), the load-displacement curves presented in Figure 6 reveal a distinct failure characterized by a sudden drop in load capacity after reaching the peak point. This sudden drop, particularly evident in model KJ0-45-46 (Figure 6a), is attributed to local buckling of the compression brace in the vicinity of the brace-to-column intersection, accompanied by significant plastification and inward deformation of the column wall at the connection zone. As the applied load increases, the steel bracing member experiences large compressive stresses at the connection point, causing deformation and shrinkage of the column tube wall. This localized deformation eventually leads to a sudden loss of load-bearing capacity, which is an undesirable failure mode. The small jump observed in the curve at a displacement of approximately 65 mm indicates the onset of local column failure, further confirming the occurrence of localized instability in the hollow models. In contrast, models with larger brace diameters (e.g., KJ0-45-85 in Figure 6b) exhibit a more gradual post-peak response, with the maximum capacity occurring at a larger displacement (48 mm) but with a lower peak load (1077 kN). This indicates that increasing the brace diameter shifts the failure mode towards earlier plastification of the column wall due to higher punching shear forces, as discussed in the following sections.

5.2 Failure Mechanisms of Models with Concrete Infill

For the models with sandwiched concrete (KJ24 series), the load-displacement curves presented in Figure 7 show a significantly different behaviour characterized by higher peak loads, greater ductility, and more gradual post-peak degradation. The presence of concrete infill effectively delays local buckling of the column wall by providing internal support to the steel tube, thereby redistributing stresses more uniformly across the joint. As a result, the failure mode in these models is either buckling of the compression brace or plastification of the column member at the brace-to-column intersection, both of which are considered desirable failure modes. The maximum load resisted by model KJ24-45-46 (Figure 7a) is 2755 kN at a displacement of 59 mm, representing a 156% increase in load capacity compared to the hollow model KJ0-45-46. This substantial improvement is attributed to the direct contribution of concrete to the compressive resistance, as well as its role in enhancing the overall stability and stiffness of the joint. Additionally, the ultimate displacement of the concrete-filled models is significantly larger than that of the hollow models, indicating superior ductility. This is evident when comparing Figure 7 (all curves) with Figure 6 (all curves), where the concrete-filled models consistently exhibit larger displacement capacities before failure.

5.3 Effect of Brace Diameter on Joint Capacity and Failure

The observed reduction in load-bearing capacity with increasing brace diameter (from 46 mm to 85 mm) can be explained through the punching shear mechanism. As the brace diameter increases, the contact area between the brace and the column wall increases, leading to a larger resultant force being transferred to the column surface. This results in higher punching shear stresses acting on the chord wall at the intersection. The increased punching shear force exceeds the local shear resistance of the column wall, causing earlier yielding and plastification of the steel tube around the weld zone. Consequently, the joint reaches its ultimate capacity at a lower load level and experiences more severe local deformation, leading to a reduction in overall load-bearing capacity. This mechanism is clearly reflected in the load-displacement curves. For instance, model KJ0-45-46 (Figure 6a) reaches a peak load of 1314 kN, while model KJ0-45-85 (Figure 6b) with a larger brace diameter shows a peak load of only 1077 kN, representing a 12% reduction. Similarly, in the concrete-filled series, model KJ24-45-46 (Figure 7a) exhibits a peak load of 2755 kN, whereas model KJ24-45-85 (Figure 7b) shows a lower peak load. It should be noted that although the presence of concrete significantly enhances the overall capacity, the detrimental effect of increasing brace diameter remains evident in both hollow and concrete-filled models.

5.4 Effect of Brace-to-Column Angle on Joint Capacity and Failure

The decrease in joint capacity with increasing brace-to-column angle (from 45° to 60°) can be attributed to the change in the force transfer mechanism. When the angle increases, the horizontal component of the brace force decreases, while the vertical component increases. This alters the load path within the joint and reduces the efficiency of force transfer from the brace to the column. The reduced horizontal component means that a smaller portion of the brace force contributes to the compressive resistance of the column, while the larger vertical component induces higher localized stresses at the connection. As a result, the joint experiences earlier yielding and plastification of the column wall at the intersection, leading to a reduction in ultimate capacity. This trend is clearly observable in the load-displacement curves. Model KJ0-45-46 (Figure 6a) exhibits a peak load of 1314 kN, while model KJ0-60-46 (Figure 6c) with a larger angle shows a peak load of only 982 kN, representing a 9% reduction. The same trend is observed in the concrete-filled series, where model KJ24-45-46 (Figure 7a) shows higher capacity compared to model KJ24-60-46 (Figure 7c). These observations confirm that connections with a smaller angle have a higher bearing capacity, which can be related to the principle of superposition of forces and the more effective contribution of brace members to the load-bearing capacity at smaller angles.

5.5 Role of Sandwiched Concrete in Enhancing Joint Behaviour

The presence of sandwiched concrete significantly improves the joint capacity and ductility through several mechanisms. First, the concrete infill provides internal confinement to the outer steel tube, delaying the onset of local buckling and enhancing the overall stability of the column member. Second, the concrete contributes directly to the load-bearing capacity by sharing the compressive stresses transferred from the brace members. Third, the concrete acts as a stress distributor, reducing the stress concentration at the weld zone and promoting a more uniform stress distribution across the joint. These combined effects are clearly demonstrated by comparing the load-displacement curves of hollow models (Figure 6) with those of concrete-filled models (Figure 7). The concrete-filled models consistently exhibit substantially higher peak loads (up to 156% increase), larger ultimate displacements, and more gradual post-peak degradation, indicating enhanced ductility and energy dissipation capacity. Furthermore, the failure mode shifts from localized column wall buckling in hollow models to either brace buckling or column plastification with concrete support in concrete-filled models, both of which are more favourable from a structural design perspective.

5.6 Summary of Parametric Effects on Joint Behaviour

Based on the mechanistic analysis of the load-displacement curves and the observed failure patterns, the following key findings are summarized: increasing the brace diameter reduces the load-bearing capacity in both hollow and concrete-filled models due to higher punching shear forces acting on the column wall; increasing the brace-to-column angle reduces the load-bearing capacity due to less effective force transfer and higher localized stresses at the connection; models without concrete infill exhibit sudden strength drops and localized column wall buckling, which are undesirable failure modes with limited ductility; models with sandwiched concrete exhibit significantly higher peak loads, greater ductility, and more favourable failure modes, demonstrating the beneficial role of concrete infill; and the maximum load capacity of 2755 kN was achieved by model KJ24-45-46, representing a 156% increase compared to the corresponding hollow model KJ0-45-46.

6. Conclusions

In this study, the load-bearing capacity of CFDST K-joints under monotonic loading was studied using the finite element method. The K-joints were modeled and analyzed parametrically using the Abaqus software. The parameters studied included the effect of increasing the diameter of the brace member on the failure behavior and overall load-bearing capacity of the K-shaped joint, as well as the change in the angle between the brace member and the main column and its effect on the load-bearing capacity of the joint. In addition, the effect of the presence and absence of sandwiched concrete in the K-joint and its contribution to the failure mode and load-bearing capacity of the joint were discussed. The following items can be expressed:

1. A small jump at the load-displacement curve in models with no sandwiched concrete shows the local failure of the column member. As such, the steel bracing member buckles and incurs a large pressure to the main column at the connection point. This causes deformation and shrinkage of this part of the joint, which is an undesirable mode of failure.
2. The load-bearing capacity of the K-joint decreases with increasing the brace diameter. In this regard, the maximum load of model KJ0-45-85 is equal to 1077 kN, which shows a reduction of 12% in the load-bearing capacity of the K-joint KJ0-45-46.
3. Increasing the angle between brace and column members reduces the load-bearing capacity. In this sense, the maximum bearing capacity of joint model KJ0-60-46 is 982 kN at a displacement of 33 mm. This indicates a reduction of 9% in the load-bearing capacity compared to joint model KJ0-45-46 with a maximum load of 1314 kN. As a result, connections with a smaller angle have a higher bearing capacity. This can be related to the principle of superposition of forces, and subsequently, the higher contribution of brace members with the column to load-bearing capacity at smaller angles.
4. Joint model KJ0-60-85 has the lowest load capacity because it bears the highest brace diameter and angle.
5. Models with sandwiched concrete have higher peak loads, compared to those with no filler concrete. This is due to the contribution of concrete to the overall capacity increase of the CFDST K-joint. In this regard, the maximum load resisted by K-joint KJ24-45-46 is 2755 kN at a displacement of 59 mm. This is indicative of a 156% increase in load capacity of the CFDST K-joint in comparison to the joint with no concrete.
6. Comparison of the ultimate displacement for models without concrete shows that the ductility of these models is much lower than that of models having concrete.
7. Although filling K-joints with concrete significantly increases the stiffness and overall capacity of the joint, the effect of concrete compressive strength itself was not parametrically investigated in this study; further research is needed to draw general conclusions.

7. Acknowledgments

The authors acknowledge the use of AI-assisted language editing tools for improving the readability and grammar of this manuscript. All technical content, analysis, results, and conclusions remain the sole responsibility of the authors.

References

[1] J. Fan, M. Xie, Y. Liu, H. Guo, J. Zhao, Seismic and numerical investigation of semi-rigid CFDST joints with flush endplates, Journal of Building Engineering, 102 (2025) 111983.
[2] M. Abbasnejadfard, M. Farzam, The effect of opening on stiffness and strength of infilled steel frames, Journal of Rehabilitation in Civil Engineering, 4(1) (2016) 78–90.
[3] O. Rezaifar, A. Yoonesi, S. Yousefi, M. Gholhaki, Analytical study of concrete-filled effect on the seismic behavior of restrained beam-column steel joints, Scientia Iranica. Transaction A, Civil Engineering, 23(2) (2016) 475.
[4] S. Savas, M. Ulker, S. Turgut, D. Bakir, Determination of energy damping upon impact load in reinforced concrete sandwich plates with different core geometries, Scientia Iranica, 28(6) (2021) 3082–3091.
[5] S. Noui, A. Kadid, A. Bali, Influence of masonry panels with openings on the seismic response of reinforced concrete infilled frames, Scientia Iranica, 26(1) (2019) 157–166.
[6] M. Mohammadi, State of the art on the maximum strength of masonry infilled frames, Scientia Iranica, 24(3) (2017) 900–909.

[7] J.-H. Fan, W.-D. Wang, Y.-L. Shi, L. Zheng, Low-cycle fatigue behaviour of concrete-filled double skin steel tubular (CFDST) members for wind turbine towers, Thin-Walled Structures, 205 (2024) 112384.
[8] L. Guo, J. Wang, W. Wang, Z. Ding, Component based moment-rotation model of composite beam blind bolted to CFDST column joint, Steel and Composite Structures, 38(5) (2021) 547–562.
[9] F. Wang, Z. Cheng, J. Shen, Flexural fatigue behavior of butt-welded circular concrete-filled double skin steel tube (CFDST): Experimental study and numerical modeling, Marine Structures, 88 (2023) 103380.
[10] N. Mahdavi, M. Salimi, M. Ghalehnovi, Experimental study of octagonal steel columns filled with plain and fiber concrete under the influence of compressive axial load with eccentricity, Journal of Rehabilitation in Civil Engineering, 9(1) (2021) 1–18.
[11] A. Karkabadi, M.I. Khodakarami, In-Plane Cyclic Response of Separated Masonry Infill Walls Using Polymeric Materials at the Surrounding Steel Frames Interface Using 3D FE Analysis, Journal of Rehabilitation in Civil Engineering, 11(3) (2023) 18–46.
[12] H. Saberi, V. Kolmi Zade, A. Mokhtari, V. Saberi, Investigating of the effect of concrete confinement on the axial performance of circular concrete filled double-skin steel tubular (CFDST) long columns, Journal of Rehabilitation in Civil Engineering, 8(3) (2020) 43–59.
[13] M.A. Eltaf, A.A. Raoufy, Seismic Resilience Enhancement of a Typical Infilled RC Frame Residential Building with Fiber Reinforced Polymer Material: A Case Study in Kabul City, Afghanistan, Journal of Rehabilitation in Civil Engineering, 13(4) (2025) 110–130.
[14] H. Tekeli, A. Aydin, An experimental study of the seismic behavior of infilled RC frames with opening, Scientia Iranica, 24(5) (2017) 2271–2282.
[15] H. Tavakoli, T. Mofid, M. Dehestani, Dynamic analysis of thermal crack propagation in roller-compacted Concrete dams considering rotational component of ground motion, Civil Engineering Infrastructures Journal, 57(2) (2024) 287–302.
[16] T. Mofid, A. Al-sharea, XFEM-Oriented Finite Element Parametric Analysis of CFRP-Retrofitted Concrete Beams Subjected to Center-Point Load, Civil Engineering Infrastructures Journal, (2026) e108404.
[17] Q. Xia, L. Ma, G. Li, C. Hu, L. Zhang, F. Xu, Z. Liu, Stress concentration factors of concrete-filled double-skin tubular K-joints, Buildings, 14(5) (2024) 1363.
[18] M. Naghipour, S.M.R. Hasani, Numerical investigation of ultimate bearing capacity of circular and square concrete-filled double steel tubular T-joints, Proceedings of the Institution of Mechanical Engineers, Part L: Journal of Materials: Design and Applications, 238(6) (2024) 1099–1113.
[19] Q. Li, X. Zhou, Y. Wang, J.B. Lim, B. Wang, S. Gao, Static performance of multi-planar CFST chord-CHS brace KK joints, Journal of Constructional Steel Research, 213 (2024) 108428.
[20] W. Huang, L. Fenu, B. Chen, B. Briseghella, Experimental study on K-joints of concrete-filled steel tubular truss structures, Journal of Constructional Steel Research, 107 (2015) 182–193.
[21] D. Witteck, R. Winkler, M. Knobloch, Experimental Investigation of Concrete-Filled Double Steel Tube Columns (CFDST) with High Performance Materials Under Monotonic and Cyclic Loading, in: International Conference on the Behaviour of Steel Structures in Seismic Areas, Springer, 2022, pp. 133–140.
[22] H. Zhao, R. Wang, D. Lam, C.-C. Hou, R. Zhang, Behaviours of circular CFDST with stainless steel external tube: Slender columns and beams, Thin-Walled Structures, 158 (2021) 107172.
[23] Z.-C. Yang, W. Li, Y.-F. Cheng, L.-H. Han, Seismic performance of grouted CFDST column base: Investigation and design method, Engineering Structures, 331 (2025) 119977.
[24] S. Asadollahi, M. Labibzadeh, F. Hosseinlou, A. Khajehdezfuly, Analytical Formula for Load-Carrying Capacity of Eccentrically Loaded CFDT Columns and Performance Comparison with CFST Columns Under Seismic Loads, Iranian Journal of Science and Technology, Transactions of Civil Engineering, 47(5) (2023) 3033–3054.
[25] T. Mofid, H. Tavakoli, Experimental investigation of mechanical behavior of lightweight RC elements under repeated loadings, in: Structures, Elsevier, 2023, pp. 1608–1622.
[26] T. Mofid, H. Tavakoli, Experimental investigation of post-earthquake behavior of RC beams, Journal of Building Engineering, 32 (2020) 101673.
[27] T. Mofid, H. Tavakoli, Experimental Investigation of Cyclic Degradation of Light RC Beams under Periodic Loading, Journal of Structural and Construction Engineering, 8(Special Issue 2) (2021) 243–263.
[28] L.-H. Han, C.-C. Hou, X.-L. Zhao, K.J. Rasmussen, Behaviour of high-strength concrete filled steel tubes under transverse impact loading, Journal of Constructional Steel Research, 92 (2014) 25–39.
[29] C. Hou, L.-H. Han, Analytical behaviour of CFDST chord to CHS brace composite K-joints, Journal of Constructional Steel Research, 128 (2017) 618–632.
[30] C. Hou, L.-H. Han, T.-M. Mu, Behaviour of CFDST chord to CHS brace composite K-joints: Experiments, Journal of Constructional Steel Research, 135 (2017) 97–109.